



Rational Design of the Platinahelicene Enantiomers for Deep-Red Circularly Polarized Organic Light-Emitting Diodes

Zhi-Ping Yan, Xu-Feng Luo, Kang Liao, You-Xuan Zheng* and Jing-Lin Zuo*

State Key Laboratory of Coordination Chemistry, Jiangsu Key Laboratory of Advanced Organic Materials, School of Chemistry and Chemical Engineering, Nanjing University, Nanjing, China

OPEN ACCESS

Edited by:

Ralph Ernstorfer,
Fritz-Haber-Institute, Germany

Reviewed by:

Yue Wang,
Jilin University, China
Wai-Yeung Wong,
Hong Kong Polytechnic University,
Hong Kong

*Correspondence:

You-Xuan Zheng
yxzheng@nju.edu.cn
Jing-Lin Zuo
zuojl@nju.edu.cn

Specialty section:

This article was submitted to
Physical Chemistry and Chemical
Physics,
a section of the journal
Frontiers in Chemistry

Received: 13 February 2020

Accepted: 15 May 2020

Published: 17 June 2020

Citation:

Yan Z-P, Luo X-F, Liao K, Zheng Y-X
and Zuo J-L (2020) Rational Design of
the Platinahelicene Enantiomers for
Deep-Red Circularly Polarized Organic
Light-Emitting Diodes.
Front. Chem. 8:501.
doi: 10.3389/fchem.2020.00501

[n]Helicene derivatives are most popular chiral structures to construct luminescent materials with circularly polarized (CP) light, which have revealed appealing application in chiral optoelectronics. Particularly, because of the unique phosphorescent emission, platinahelicene has great application prospects in CP organic light-emitting diode (CP-OLED). Herein, by decorating the pyridinyl-helicene ligand with trifluoromethyl (-CF₃) unit in a specific position, a pair of platinahelicene enantiomers was prepared and separated with extremely twisted structure showing not only superior thermal and configurational stability but also good CP luminescence (CPL) property with dissymmetry factors ($|g_{PL}|$) of 6×10^{-3} . Moreover, the evaporated CP-OLEDs based on platinahelicene enantiomers exhibited the deep-red emission with the peak at 653 nm as well as obvious CP electroluminescence (CPEL) signals with the $|g_{EL}|$ in 10^{-3} order. Therefore, the design strategy provides an efficient way to improve the CPL properties of platinahelicene to cope with the future application in CP-OLEDs.

Keywords: platinahelicene, circularly polarized light, thermal and configurational stability, CP-OLED, deep-red emission

INTRODUCTION

In recent years, the exploration of chiral materials enabling circularly polarized (CP) light has attracted widespread attention in the field of chiral optoelectronics (Zhang et al., 2014). Compared with the traditional way of obtaining CP light (Grell et al., 2001) with polarizer, CP organic light-emitting diodes (CP-OLEDs) (Li et al., 2015, 2018) could emit CP light directly, which avoid brightness loss and complicated device structures. In term of current research (Han et al., 2018), it is still an important way to design chiral materials with excellent CPL properties for achieving high-performance CP-OLEDs. And the degree of circularly polarized photoluminescence (CPPL) or circularly polarized electroluminescence (CPEL) is characterized by the dissymmetry factor (g_{PL} or g_{EL}) defined as $g = 2 \times \Delta I / I = 2 \times (I_L - I_R) / (I_L + I_R)$. For example, Meijer and co-workers (Peeters et al., 1997) firstly obtained CP electroluminescence (CPEL) by using a chiral-substituted poly(p-phenylenevinylene) derivative as emitter. Since then, there has been some progress in chiral luminescent materials and efficient CP-OLEDs. Notably, although several reported chiral lanthanide complexes (Zinna et al., 2015, 2017) show excellent CPL properties with the $|g_{PL}|$ values over 1, the poor device performances make them difficult to be applied for practical OLEDs. On the contrary, chiral transition metal complexes [Ir(III), Pt(II)] and thermally activated delayed

Scientific) and Matrix Assisted Laser Desorption Ionization Time of Flight Mass Spectrometry (autoflex TOF/TOF, Bruker Daltonics), high-resolution mass spectra were recorded on a MICROTOF-Q III instrument. Ultraviolet-visible (UV-vis) absorption spectra were measured on a UV-3100 spectrophotometer and PL spectra were obtained from a Hitachi F-4600 photoluminescence spectrophotometer. The absolute photoluminescence quantum yields (Φ) and the decay lifetimes of the complex were measured by HORIBA FL-3 fluorescence spectrometer. Thermogravimetric analysis (TGA) was performed on a Pyris 1 DSC under nitrogen at a heating rate of $10^{\circ}\text{C min}^{-1}$. (RAC)-Pt was separated by CHIRALPAK IE (IE00CD-RH008) column which was employed as stationary phase and the hexane/dichloromethane (80/20) was employed as eluent. Cyclic-voltammetry measurement system carried out at room temperature in deaerated CH_3CN , employing a polished Pt plate as the working electrode, terta-n-butylammonium perchlorate (0.1 M) as the supporting electrolyte and Fc^+/Fc used as the reference, with the scan rate of 0.1 V/s. The HOMO and LUMO levels were obtained by the following equation: $E_{\text{HOMO}} = -(4.8 + E_{\text{oxonset}})$ (eV), $E_{\text{LUMO}} = -(E_{\text{HOMO}} + E_{\text{g}})$ (eV), and E_{g} was estimated from the UV-vis absorption spectra, $E_{\text{g}} = hc/\lambda_{\text{abs}}$. The circular dichroism (CD) and CPL spectra were measured in the same condition with UV-Vis absorption spectra and PL spectra. The CD spectra were measured on a Jasco J-810 circular dichroism spectrometer with “low” sensitivity. The circularly polarized photoluminescence (CPPL) and circularly polarized electroluminescence (CPEL) spectra were measured on a Jasco CPL-300 spectrophotometer based on “Continuous”

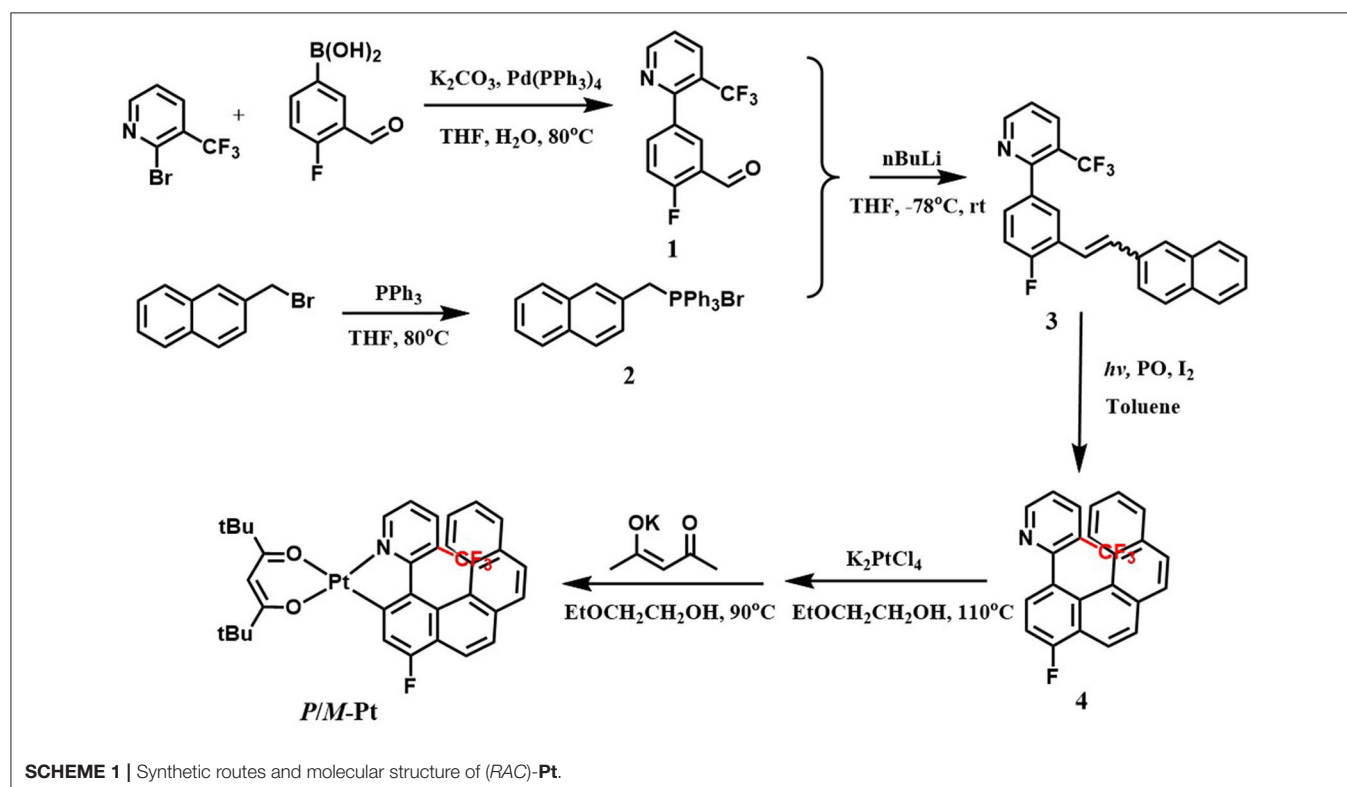
scanning mode at 200 nm/min scan speed. The test mode adopts “Slit” mode with the E_x and E_m Slit width $3,000 \mu\text{m}$ and the digital integration time (D.I.T.) is 2.0 s with multiple accumulations (10 times or more).

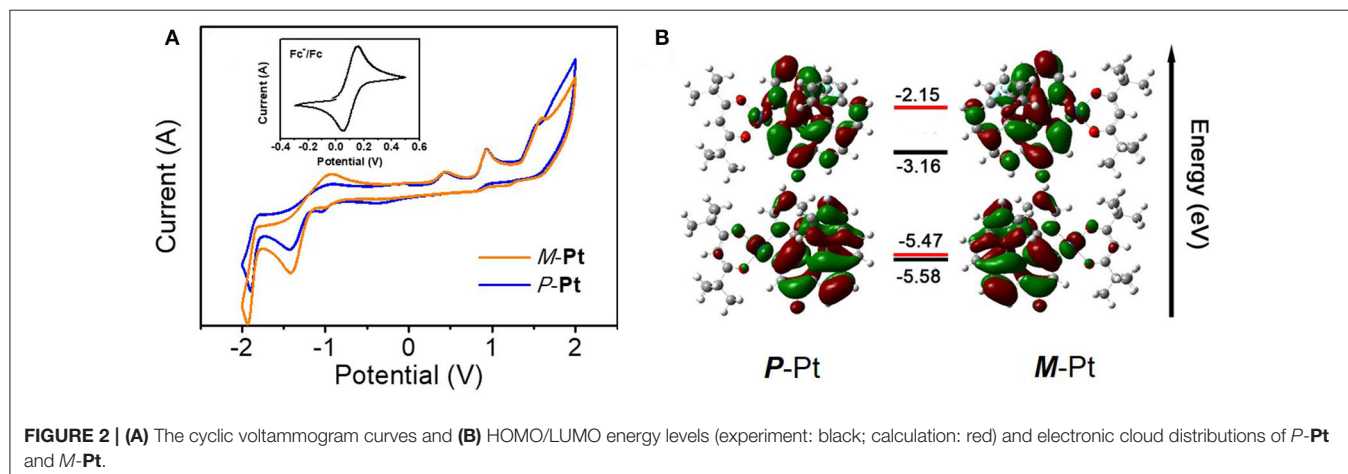
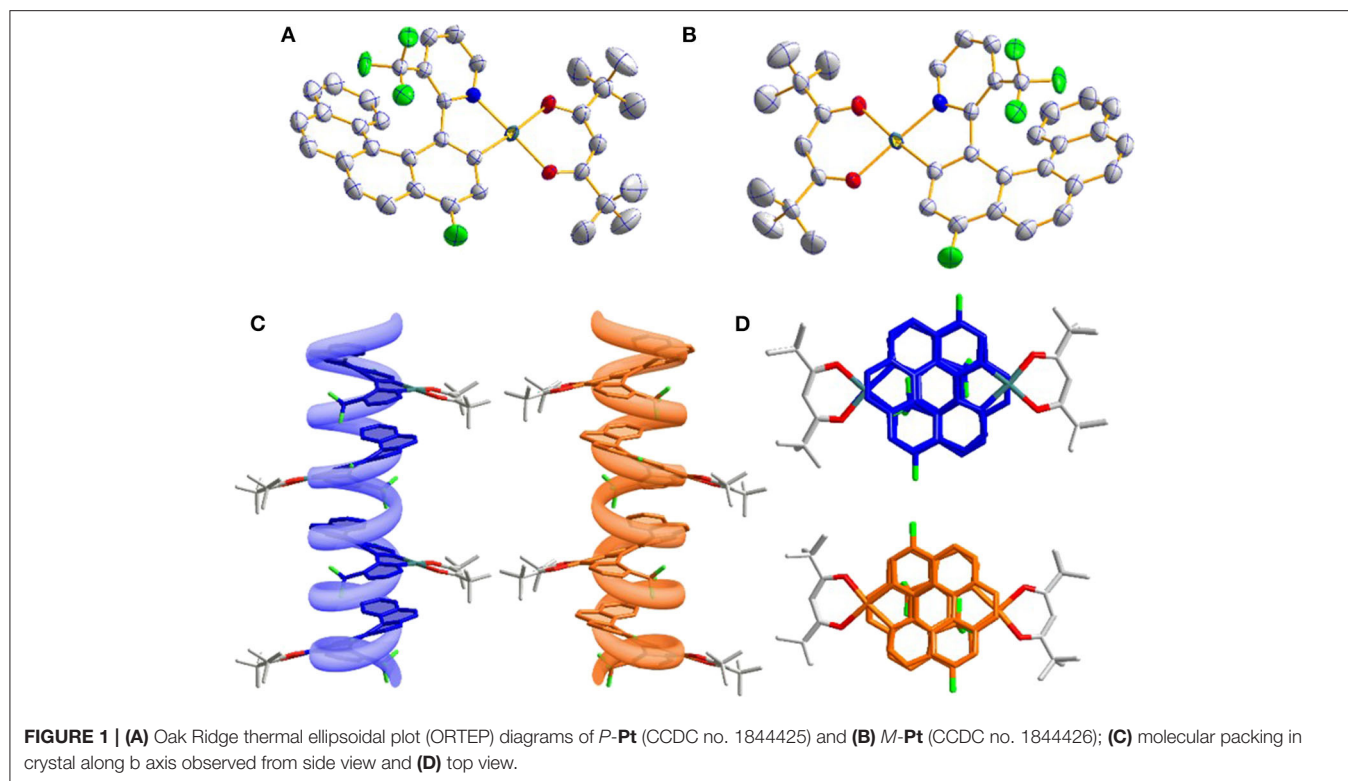
Theoretical Calculation

All the DFT and TD-DFT calculations were carried out using Gaussian 16 software package. The initial structures were created according to the GaussView 6 based on crystal structures. The ground state geometry optimization with frequent calculations for all the complexes were performed using B3LYP exchange-correlation functional. On the basis of the optimized structures, vertical transition energy calculations were carried out with B3LYP functional, too. For all the calculations, a combination of basis sets that Lanl2dz for platinum and 6-31G (d,p) for the others were employed and the solvent effect were considered by C-PCM model in CH_2Cl_2 .

Device Fabrication

All the final products were purified by sublimation before applied to device fabrication. Moreover, the OLEDs with the emission area of 0.1 cm^2 were fabricated on the pre-patterned ITO-coated glass substrate with a sheet resistance of $15 \Omega \text{ sq}^{-1}$. The ITO glass substrates were cleaned with ITO lotion and deionized water and then dried in an oven at 120°C . The devices were fabricated by vacuum deposition of the materials at $<10^{-4} \text{ Pa}$ with the deposition rate of $1\text{--}2 \text{ \AA s}^{-1}$. The platinahelicene and host were co-evaporated from two separate sources. The LiF and Al were deposited with the rate of 0.1 and 3 \AA s^{-1} , respectively.





RESULT AND DISCUSSION

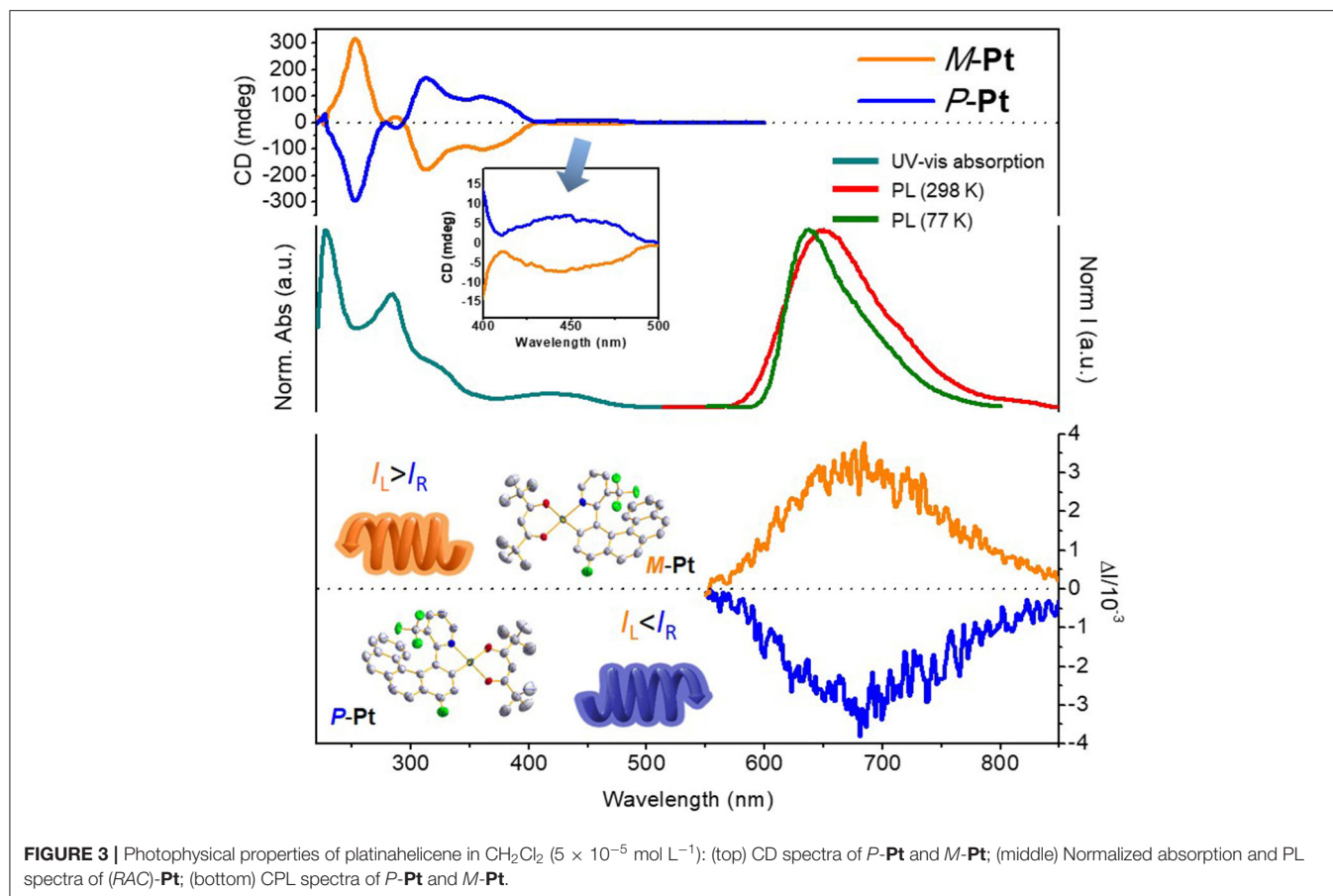
Preparation and Characterization of Platinahelicene

All experiments were performed under nitrogen atmosphere and the relevant procedures referred to the reported literature (Norel et al., 2010). The starting reactants and solvents were used as commercial grade without further purification. The synthetic routes of (*RAC*)-Pt are depicted in **Scheme 1**. The helicene ligand **4** and (C^N)Pt(μ -Cl) chloride-bridged dimer were prepared by the reported methods. Then the platinahelicene was readily obtained by mixing the μ -chloro-bridged dimer with 2,2,6,6-tetramethylheptane-3,5-dione sodium salt. The target platinahelicene was purified by column

chromatography and sublimation. Due to the rapid racemization at room temperature, the helicene ligand is difficult to be separated into stable enantiomers. On the contrary, with the introduction of coordination bond, *P*-Pt and *M*-Pt are configurationally stable, which could be separated by (*RAC*)-Pt by using chiral HPLC with enantiomeric purity higher than 99%.

1-Fluoro-4-(6-Trifluoromethyl-2-Pyridyl)-Benzo[*g*]Phenanthrene (**4**)

The mixture of *cis* and *trans* **3** (1.0 g, 2.55 mmol), I_2 (30 mg, 0.12 mmol) and 10 ml propylene oxide were dissolved in toluene (1,000 mL). The solution was irradiated for 4 h by 250 W mercury



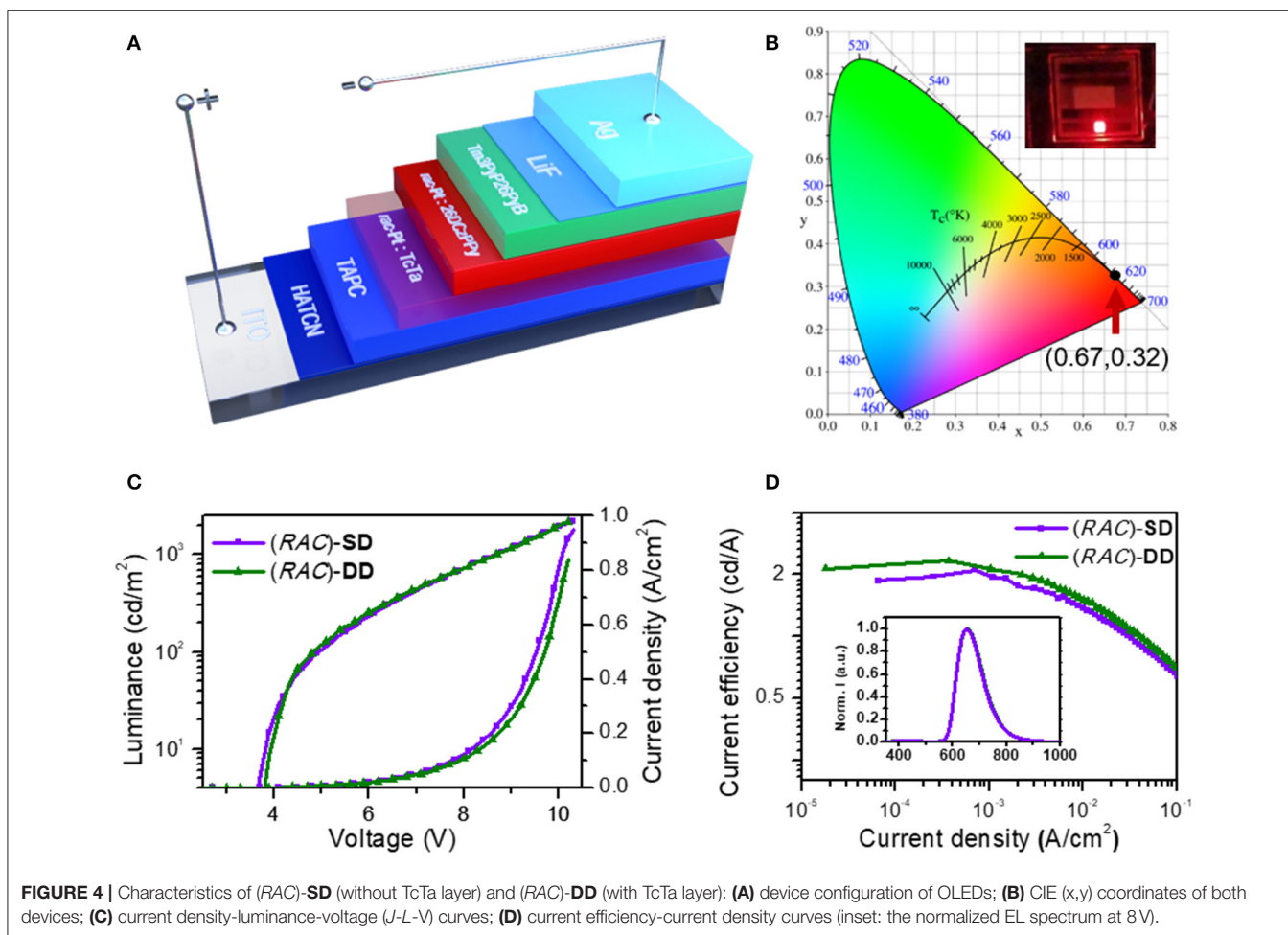
vapor lamps. The solvent was evaporated under reduced pressure and then the residue was purified by column chromatography [silica gel, ethyl acetate: petroleum ether 1:10 (v/v)] to afford **4** as a beige solid (598 mg, 60%). ESI-MS, calculated: m/z 392.11 for $[\text{M}+\text{H}]^+$ ($\text{C}_{24}\text{H}_{14}\text{F}_4\text{N}$) $^+$ found: m/z 392.25. ^1H NMR (400 MHz, CDCl_3): δ 9.05 (d, $J = 3.7$ Hz, 1H), 8.27 (d, $J = 8.6$ Hz, 1H), 8.03 (dd, $J = 19.2, 8.1$ Hz, 1H), 7.92 (dt, $J = 8.4, 4.3$ Hz, 2H), 7.89–7.77 (m, 3H), 7.72 (d, $J = 8.0$ Hz, 1H), 7.44 (dt, $J = 31.7, 8.8$ Hz, 1H), 7.30 (d, $J = 7.8$ Hz, 1H), 7.22 (t, $J = 7.4$ Hz, 1H), 6.99 (t, $J = 7.3$ Hz, 1H).

(6-Trifluoromethyl-2-[4'-(1'-fluorobenzo[*g*]phenanthrenyl)]pyridinato-*N*, *C*)platinum-*tert*-butylacetylacetonate (*RAC*)-Pt

1) Preparation of the platinum μ -chloro-bridged dimer: To a solution of **4** (400 mg, 1.02 mmol) in ethoxyethanol (30 mL) was added K_2PtCl_4 (423 mg, 1.02 mmol). The suspension was gently warmed with stirring until all the platinum salt dissolved. The solution was then refluxed for 16 h to yield a dark green suspension. After cooled to room temperature, water (100 mL) was added. The precipitation was filtered and dried in air and then dark yellow solid (549 mg, 88%) was obtained.

2) Preparation of (*RAC*)-Pt: To a solution of μ -chloro-bridged dimer (549 mg, 0.44 mmol) in ethoxyethanol (25 mL) was added the 2,2,6,6-tetramethylheptane-3,5-dione sodium salt (217 mg, 0.97 mmol). The reaction mixture was refluxed overnight and then concentrated under reduced pressure. Purification by column chromatography (silica gel, ethyl acetate: petroleum ether 1:4 (v/v)), yielded (*RAC*)-Pt as orange-red solid (337 mg, 50%). MALDI-TOF-MS, calculated: 768.194 for *M* ($\text{C}_{35}\text{H}_{31}\text{F}_4\text{NO}_2\text{Pt}$), found: 768.382; HR-MS, calculated: 769.2011 for $[\text{M}+\text{H}]^+$ ($\text{C}_{35}\text{H}_{32}\text{F}_4\text{NO}_2\text{Pt}$) $^+$, found: 769.2013. ^1H NMR (400 MHz, CDCl_3): δ 9.25 (d, $J = 4.6$ Hz, 1H), 8.21 (d, $J = 8.5$ Hz, 1H), 8.11 (d, $J = 8.5$ Hz, 1H), 7.84 (q, $J = 8.6$ Hz, 2H), 7.79 (dd, $J = 8.0, 5.1$ Hz, 2H), 7.58 (d, $J = 9.3$ Hz, 1H), 7.34 (d, $J = 6.9$ Hz, 1H), 7.24 (t, $J = 7.3$ Hz, 1H), 7.05–6.99 (m, 1H), 6.92 (t, $J = 7.7$ Hz, 1H), 5.91 (s, 1H), 1.34 (d, $J = 6.2$ Hz, 18H).

The single crystals of two enantiomers were obtained by vacuum sublimation and the single crystal diffraction analysis further confirmed the preconceived structure. As shown in **Figures 1A, 5B**, two symmetric enantiomers adopted twisted planar structures could be easily divided into *P* and *M* configurations. Interestingly, because the $-\text{CF}_3$ group is inserted into the helicene-like skeleton, the twist angle of pyridine and the coordinate five-membered rings is 17.3° , bigger than the relevant report (Norel et al., 2010; Yan et al., 2019a), and the consecutive twist angles between the fused rings (10.6, 12.1, 12.3,



and 9.9°) lead to a helical curvature (hc , the angle between the terminal helicene rings) value of 38.7° in *P*-Pt and *M*-Pt, which is smaller than the conventional organic or heteroatomic [6]helicene system (Graule et al., 2009). Although the helicene-based ligand shows a large distortion, the central Pt(II) still adopts a planar coordination form with the dihedral angle 5° between plane O_1 -Pt- O_2 and N_1 -Pt- C_1 . Moreover, the smaller hc value leads to relative strong π - π interactions, as a result, *P*-Pt and *M*-Pt pile up in a parallel face-to-face style. As shown in **Figures 1C,D**, combining with the help of the special chiral *P* or *M* helicene unit, these strong interactions can self-assemble *P*-Pt and *M*-Pt to form *P* and *M* spiral structures, which may be a reason of the good CPL properties of the platinahelicene.

Thermal and Configurational Stability

Thermal and configurational stability was investigated by TGA and CD spectra, respectively, which are vital parameters for chiral materials to fabricate CP-OLEDs. As shown in **Figure S12**, the decomposition temperature (T_d , 5% loss of weight) of (RAC)-Pt is 321°C , which benefits the application during the operation of CP-OLEDs. Moreover, due to the introduction of large sterically hindered groups, these enantiomers are endowed with a better configurational stability, which could preserve the

TABLE 1 | EL performances of the devices based on (RAC)-Pt, *P*-Pt, and *M*-Pt.

| Device | V_{on}^a [V] | L_{max}^b [cd/m ²] | $\eta_{\text{c,max}}^c$ [cd/A] | $\eta_{\text{c,L1000}}^d$ [cd/A] | $\text{EQE}_{\text{max}}^e$ [%] | $\eta_{\text{p,max}}^f$ [lm/W] | g_{EL}^g [10 ⁻³] |
|--------------|--------------------------|--|-----------------------------------|-------------------------------------|------------------------------------|-----------------------------------|--|
| (RAC)-SD | 3.6 | 2,222 | 2.29 | 0.47 | 4.16 | 1.90 | – |
| (RAC)-DD | 3.6 | 2,201 | 2.33 | 0.52 | 4.44 | 1.88 | – |
| <i>P</i> -SD | 3.4 | 1,927 | 2.26 | 0.47 | 4.42 | 2.03 | -1.1 |
| <i>M</i> -SD | 3.4 | 2,156 | 2.14 | 0.36 | 4.17 | 1.91 | 1.1 |
| <i>P</i> -DD | 3.6 | 1,754 | 2.23 | 0.47 | 4.06 | 1.87 | -0.9 |
| <i>M</i> -DD | 3.6 | 1,840 | 2.32 | 0.48 | 4.60 | 1.97 | 1.3 |

^aTurn-on voltage recorded at a luminance of 1 cd/m²; ^bMaximum luminance; ^cMaximum current efficiency; ^dCurrent efficiency at 1,000 cd/m²; ^eMaximum external quantum efficiency; ^fMaximum power efficiency; ^g g_{EL} around maximum emission peak.

original configuration (**Figure S11**) even at 240°C under vacuum of 1×10^{-4} Pa overnight.

Electrochemical Property and Theoretical Calculation

Cyclic voltammetry (CV) measurements and density functional theory (DFT) calculations were further conducted to investigate

the electronic and structural features of *P*-Pt and *M*-Pt. As depicted in **Figure 2A**, both complexes have irreversible oxidation and reduction waves and the electrochemical data are summarized in **Table S3**. The oxidation onsets of these two enantiomers reference Fc^+/Fc are the same with the value of 0.78 V. Moreover, both *P*-Pt and *M*-Pt display the first reduction potential at about -1.43 V. These results demonstrated the chiral configuration has ignored influence on the electrochemical properties of the enantiomers. Therefore, the calculated highest occupied molecular orbital (HOMO) and the lowest unoccupied molecular orbital (LUMO) levels for *P*-Pt and *M*-Pt are $-5.58/-3.24$ eV, respectively, which are helpful for the carriers' injection and transport in OLEDs.

To gain a better insight of the electron cloud distributions and structure features, the molecular simulations were further executed by density functional theory (DFT) preformed with Gaussian 09 software, and the accurate energy and location of HOMO/LUMO were calculated by QMForge program. As shown in **Figure 2B**, the HOMO/LUMO are mainly distributed in the helicene ligand (77.09/91.51%) together with *d* orbitals of Pt atom (18.11/6.64%), respectively. Obviously, the distributions of HOMO/LUMO on ancillary ligand are very small, indicating the little influence on the energy level of this Pt(II) complex.

Photophysical Property

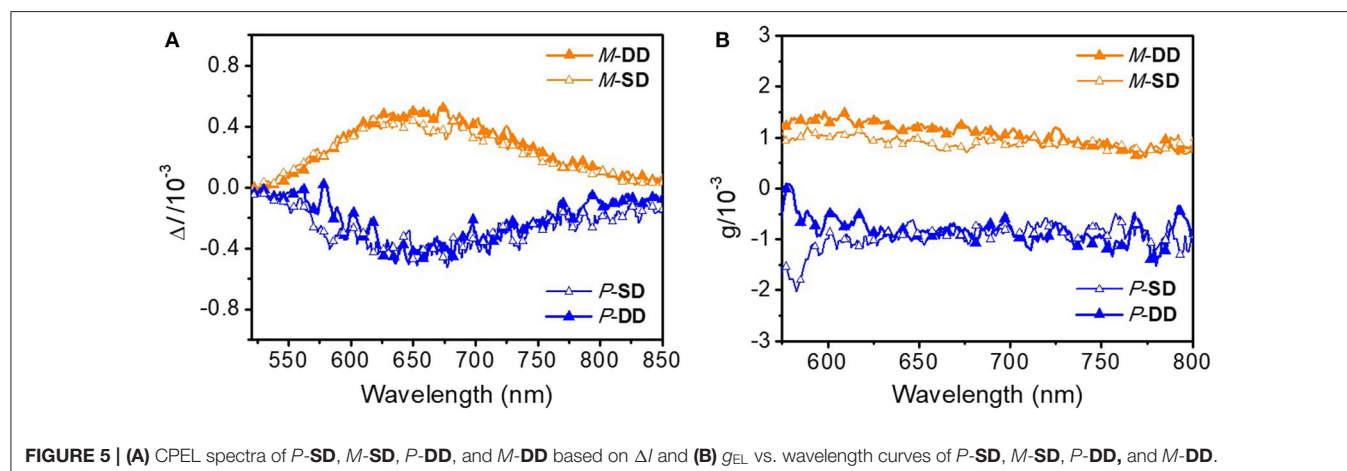
To clarify the photophysical properties of (*RAC*)-Pt, room temperature UV-vis absorption spectrum in CH_2Cl_2 is depicted in **Figure 3** (middle). The short-wavelength absorption bands at 227 and 284 nm are mainly associated with $\pi-\pi^*$ transition, while the weak absorption bands peaking at 350–500 nm would be attributed to the mixed singlet and triplet metal-to-ligand charge transfer ($^1\text{MLCT}$ and $^3\text{MLCT}$) transitions because of the strong spin-orbital coupling effect of the Pt atom. The room temperature PL spectrum of (*RAC*)-Pt was further studied with the emission peak at 650 nm and the Commission Internationale de L'Éclairage (CIE) coordinates of (0.68, 0.32) demonstrating the deep-red emission. When measured at 77 K, the emission peak has a blue shift of 14 nm with the emission peak at 636 nm.

Furthermore, emission lifetime (τ) and absolute photoluminescence quantum yield (PLQY) were recorded for (*RAC*)-Pt in CH_2Cl_2 under nitrogen atmosphere. The phosphorescence lifetime of (*RAC*)-Pt ($\tau = 4.6$ μs) is in range of the similar reported Pt(II) complexes (Shen et al., 2014). Moreover, as shown in **Figure S9**, the linear fit curve on logarithmic scale indicates the phosphorescent emission is basically the only pathway. But due to the deep-red emission with tail to the near-infrared region, the PLQY of (*RAC*)-Pt is only about 4%.

Chiroptical Property

CD spectra were reported for both enantiomers *P*-Pt and *M*-Pt in CH_2Cl_2 . As depicted in **Figure 3** (top), *P*-Pt shows a strong negative cotton effect at 249 nm and positive cotton effects at 313, 363 and 446 nm, as well as corresponding to the UV-Vis absorption spectrum. The *M*-Pt reveals exactly the opposite CD spectrum further indicating that the two components are a pair of enantiomers. Furthermore, in the range of 350–500 nm, relatively weak cotton effect is observed, indicating the circular dichroism of the MLCT process.

CPL spectra of *P*-Pt and *M*-Pt were also preformed [**Figure 3** (bottom)] to prove the chiroptical properties of the luminescent molecular upon excitations. The *P*-Pt shows negative CPL signals in 550–850 nm region while the *M*-Pt shows symmetrical signals in the same position with the $|g_{\text{PL}}|$ of about 6.0×10^{-3} which is superior compared with the reported chiral Pt(II) complexes (Shen et al., 2014; Fu et al., 2019). In order to explore the application of materials in OLEDs, the CPL properties of *P*-Pt and *M*-Pt in doped films were also investigated. When the enantiomers were doped into the host material 26DCzPPy (2,6-bis(3-(9H-carbazol-9-yl)phenyl)pyridine) at a concentration of 5 wt% by vacuum evaporation, the $|g_{\text{PL}}|$ factors are smaller than that in the solution state with the values about 4.0×10^{-3} . Apparently, as for the CPL performance of *P/M*-Pt, the host material 26DCzPPy has a certain weakening effect. However, in order to obtain better device performance, 26DCzPPy was selected to further fabricate OLED owing to its unique bipolar characteristic.



CP-OLED Characterization

Inspired by the unique phosphorescent emission, good thermal and configurational stability and chiroptical property, the application of these platinahelicene in the circularly polarized electroluminescent devices were also investigated. Considering the similar properties of enantiomers and racemate, initially (*RAC*)-Pt, was chosen to optimize the device structures. After reasonable structural optimization, the device adopting the single emissive layer of ITO/ HATCN (hexaazatriphenylene-hexacarbonitrile, 6 nm)/HATCN (0.2 wt%): TAPC (di-(4-(*N,N*-ditolyl-amino)phenyl)cyclohexane, 50 nm)/(*RAC*)-Pt (5 wt%): 26DCzPPy (10 nm)/Tm3PyP26PyB (1,3,5-*tris*(6-(3-(pyridin-3-yl)phenyl)pyridin-2-yl)benzene, 60 nm)/LiF (1 nm)/Al (100 nm) named (*RAC*)-SD showed the best performances (Figure 4A, Figure S13). Respectively, HATCN and LiF are served as the hole-injection and the electron-injection layers; TAPC and Tm3PyP26PyB are used as hole-transporting and electron-transporting layers; Bipolar 26DCzPPy is used as host material which could transport both hole and electrons. Meanwhile, trace HATCN co-doped with TAPC could reduce hole-injection potential energy to achieve low turn-on voltage. The EL spectra, luminance-voltage-current density (*L-V-J*) and current efficiency-current density characteristics of (*RAC*)-SD are depicted in Figure 4, and the key device data are summarized in Table 1. The device (*RAC*)-SD displays deep-red EL emission with the peak at 653 nm and the CIEs of (0.67, 0.32) are attained. Moreover, the turn-on voltage of (*RAC*)-SD is 3.6 V with the L_{\max} , $\eta_{c,\max}$, maximum external quantum efficiency (EQE_{\max}) and maximum power efficiency ($\eta_{p,\max}$) of 2,222 cd/m², 2.29 cd/A, 4.16% and 1.90 lm/W, respectively. Furthermore, in order to obtain better device performances, the double emissive layers device of ITO/ HATCN/ HATCN (0.2 wt%): TAPC (50 nm)/(*RAC*)-Pt (5 wt%): TcTa (4,4',4''-tris(carbazol-9-yl)triphenylamine, 10 nm)/ (*RAC*)-Pt (5 wt%): 26DCzPPy (10 nm)/Tm3PyP26PyB (60 nm)/LiF (1 nm)/Al (100 nm) named (*RAC*)-DD was also fabricated. Generally, the introduction of TcTa to fabricate double emissive layers device could broaden electron-hole recombination area which would enhance the use of electron-hole pairs. As a result, there is a certain improvement of the device performances with the L_{\max} of 2,201 cd/m², $\eta_{c,\max}$ of 2.33 cd/A, EQE_{\max} of 4.44% and $\eta_{p,\max}$ of 1.88 lm/W, respectively.

Notably, as shown in Figure 5, the two different enantiomer-based OLEDs show obvious CPEL properties with opposite g_{EL} of -1×10^{-3} and 1×10^{-3} at 653 nm for *P*-Pt and *M*-Pt, respectively, which demonstrate the successful preparation of CP-OLEDs and the device performances of *P*-SD, *M*-SD, *P*-DD, and *M*-DD are listed in Table 1 and Figure S13. Notably, although the device performance of

P-SD shows better performance at low current density, *P*-DD with wider recombination area performs better at higher current density. However, it is obvious that the measured $|g_{\text{EL}}|$ factors are smaller than the chiral material in solution and film. The reason may be the reflected circularly polarized electroluminescence from metal electrode causing the spiral direction of CP light reverse which impair the intensity of CPEL (Zinna et al., 2017; Yan et al., 2019a). Anyway, successfully obtained CPEL signals indicate a feasible way to fabricate evaporated CP-OLEDs. Meanwhile, appropriate host material and device structure may also be required for better CPEL and EL performances.

CONCLUSION

In summary, a pair of chiral platinahelicene enantiomers with excellent thermal and configurational stability was designed and synthesized. Meanwhile, owing to the special structure design strategy, *P*-Pt and *M*-Pt show good CPL properties possessing $|g_{\text{PL}}|$ of 6.0×10^{-3} in solution and 4.0×10^{-3} in doped film, respectively. And the fabricated devices *P*-SD, *M*-SD, *P*-DD, and *M*-DD exhibited deep-red emission with the emission peak around 653 nm and the EQE_{\max} of 4.6% as well as the $|g_{\text{EL}}|$ on the order of 10^{-3} .

DATA AVAILABILITY STATEMENT

All datasets generated for this study are included in the article/Supplementary Material.

AUTHOR CONTRIBUTIONS

Z-PY designed and synthesized the platinahelicene complexes, carried out relevant measurement, and wrote the manuscript. X-FL helped in material synthesis and purification. KL helped in the theoretical calculation. Y-XZ and J-LZ designed the whole research.

ACKNOWLEDGMENTS

We gratefully acknowledge the financial support from the National Natural Science Foundation of China (51773088, 21975119).

SUPPLEMENTARY MATERIAL

The Supplementary Material for this article can be found online at: <https://www.frontiersin.org/articles/10.3389/fchem.2020.00501/full#supplementary-material>

REFERENCES

Brandt, J., Wang, X., Yang, Y., Campbell, A., and Fuchter, M. (2016). Circularly polarized phosphorescent electroluminescence with a high dissymmetry factor

from PHOLEDs based on a platinahelicene. *J. Am. Chem. Soc.* 138, 9743–9746. doi: 10.1021/jacs.6b02463

Dhbaibi, K., Favereau, L., and Crassous, J. (2019). Enantioenriched helicenes and heliceneoids containing main-group elements (B, Si,

- N, P). *Chem. Rev.* 119, 8846–8953. doi: 10.1021/acs.chemrev.9b00033
- Feuillastre, S., Pauton, M., Gao, L., Desmarchelier, A., Riives, A. J., Prim, D., et al. (2016). Design and synthesis of new circularly polarized thermally activated delayed fluorescence emitters. *J. Am. Chem. Soc.* 138, 3990–3993. doi: 10.1021/jacs.6b00850
- Fu, G., He, Y., Li, W., Wang, B., Lü, X., He, H., et al. (2019). Efficient polymer light-emitting diodes (PLEDs) based on chiral [Pt(C^N)(N^O)] complexes with near-infrared (NIR) luminescence and circularly polarized (CP) light. *J. Mater. Chem. C* 7, 13743–13747. doi: 10.1039/C9TC04792A
- Graule, S., Rudolph, M., Vanthuyne, N., Autschbach, J., Roussel, C., Crassous, J., et al. (2009). Metal-bis(helicene) assemblies incorporating π -conjugated phosphole-azahelicene ligands: impacting chiroptical properties by metal variation. *J. Am. Chem. Soc.* 131, 3183–3185. doi: 10.1021/ja809396f
- Grell, M., Oda, M., Whitehead, K. S., Asimakis, A., Neher, D., and Bradley, D. D. C. (2001). A compact device for the efficient, electrically driven generation of highly circularly polarized light. *Adv. Mater.* 13, 577–580. doi: 10.1002/1521-4095(200104)13:8<577::AID-ADMA577>3.0.CO;2-K
- Han, J., Guo, S., Lu, H., Liu, S. J., Zhao, Q., and Huang, W. (2018). Recent progress on circularly polarized luminescent materials for organic optoelectronic devices. *Adv. Opt. Mater.* 6:1800538. doi: 10.1002/adom.201800538
- Han, J., Guo, S., Wang, J., Wei, L., Zhuang, Y., Liu, S., et al. (2017). Circularly polarized phosphorescent electroluminescence from chiral cationic iridium(III) isocyanide complexes. *Adv. Optical Mater.* 5:1700359. doi: 10.1002/adom.201700359
- Hellou, N., Srebro-Hooper, M., Favereau, L., Zinna, F., Caytan, E., Toupet, L., et al. (2017). Enantiopure cycloiridiated complexes bearing a pentahelicene N-Heterocyclic carbene and displaying long-lived circularly polarized phosphorescence. *Angew. Chem. Int. Ed.* 56, 8236–8239. doi: 10.1002/anie.201704263
- Li, M., Li, S. H., Zhang, D., Cai, M., Duan, L., and Fung, M. K. (2018). Stable enantiomers displaying thermally activated delayed fluorescence: efficient OLEDs with circularly polarized electroluminescence. *Angew. Chem. Int. Ed.* 57, 2889–2893. doi: 10.1002/anie.201800198
- Li, T. Y., Jing, Y. M., Liu, X., Zhao, Y., Shi, L., Tang, Z., et al. (2015). Circularly polarised phosphorescent photoluminescence and electroluminescence of iridium complexes. *Sci. Rep.* 5:14912. doi: 10.1038/srep14912
- Norel, L., Rudolph, M., Vanthuyne, N., Gareth. Williams, J. A., Lescop, C., Roussel, C., et al. (2010). Metallahelicenes: easily accessible helicene derivatives with large and tunable chiroptical properties. *Angew. Chem. Int. Ed.* 49, 99–102. doi: 10.1002/anie.200905099
- Peeters, E., Christiaans, M., Janssen, R., Schoo, H., Dekkers, H., and Meijer, E. W. (1997). Circularly polarized electroluminescence from a polymer light-emitting diode. *J. Am. Chem. Soc.* 119, 9909–10. doi: 10.1021/ja971912c
- Sakai, H., Shinto, S., Kumar, J., Araki, Y., Sakanoue, T., Takenobu, T., et al. (2015). Highly fluorescent [7]carbohelicene fused by asymmetric 1,2-dialkyl-substituted quinoxaline for circularly polarized luminescence and electroluminescence. *J. Phys. Chem. C* 119, 13937–13947. doi: 10.1021/acs.jpcc.5b03386
- Sánchez-Carnerero, E., Agarrabeitia, A., Moreno, F., Maroto, B., Muller, G., Ortiz, M., et al. (2015). Circularly polarized luminescence from simple organic molecules. *Chem. Eur. J.* 21, 13488–13500. doi: 10.1002/chem.201501178
- Shen, C., Anger, E., Srebro, M., Vanthuyne, N., Deol, K. K., Jefferson, T. D., et al. (2014). Straightforward access to mono- and bis-cycloplatinated helicenes displaying circularly polarized phosphorescence by using crystallization resolution methods. *Chem. Sci.* 5, 1915–1927. doi: 10.1039/c3sc53442a
- Wu, Z. G., Han, H. B., Yan, Z. P., Luo, X. F., Wang, Y., Zheng, Y. X., et al. (2019). Chiral octahydro-binaphthol compound-based thermally activated delayed fluorescence materials for circularly polarized electroluminescence with superior EQE of 32.6% and extremely low efficiency roll-off. *Adv. Mater.* 31:1900524. doi: 10.1002/adma.201900524
- Yan, Z. P., Liao, K., Han, H. B., Su, J., Zheng, Y. X., and Zuo, J. L. (2019b). Chiral iridium(III) complexes with four-membered Ir-S-P-S chelating rings for high-performance circularly polarized OLEDs. *Chem. Commun.* 55, 8215–8218. doi: 10.1039/C9CC03915E
- Yan, Z. P., Luo, X. F., Liu, W. Q., Wu, Z. G., Liang, X., Liao, K., et al. (2019a). Configurationally stable platinahelicene enantiomers for efficient circularly polarized phosphorescent organic light-emitting diodes. *Chem. Eur. J.* 25, 5672–5676. doi: 10.1002/chem.201900955
- Zhang, Y. J., Oka, T., Suzuki, R., and Ye, J. T. (2014). Electrically switchable chiral light-emitting transistor. *Science* 344, 725–728. doi: 10.1126/science.1251329
- Zhao, W. L., Li, M., Lu, H. Y., and Chen, C. F. (2019). Advances in helicene derivatives with circularly polarized luminescence. *Chem. Commun.* 55, 13793–13803. doi: 10.1039/C9CC06861A
- Zinna, F., Giovannella, U., and Bari, D. (2015). Highly circularly polarized electroluminescence from a chiral europium complex. *Adv. Mater.* 27, 1791–1795. doi: 10.1002/adma.201404891
- Zinna, F., Pasini, M., Galeotti, F., Botta, C., Bari, L. D., and Giovannella, U. (2017). Design of lanthanide-based OLEDs with remarkable circularly polarized electroluminescence. *Adv. Funct. Mater.* 27:1603719. doi: 10.1002/adfm.201603719

Conflict of Interest: The authors declare that the research was conducted in the absence of any commercial or financial relationships that could be construed as a potential conflict of interest.

Copyright © 2020 Yan, Luo, Liao, Zheng and Zuo. This is an open-access article distributed under the terms of the Creative Commons Attribution License (CC BY). The use, distribution or reproduction in other forums is permitted, provided the original author(s) and the copyright owner(s) are credited and that the original publication in this journal is cited, in accordance with accepted academic practice. No use, distribution or reproduction is permitted which does not comply with these terms.